scientific reports

OPEN

Naphthyridine derived colorimetric and fluorescent *turn off* sensors for Ni²⁺ in aqueous media

Abida Ashraf[1], Muhammad Islam[1], Muhammad Khalid[2✉], Anthony P. Davis[3], Muhammad Tayyeb Ahsan[1], Muhammad Yaqub[1], Asad Syed[4], Abdallah M. Elgorban[4], Ali H. Bahkali[4] & Zahid Shafiq[1✉]

Highly selective and sensitive 2,7-naphthyridine based colorimetric and fluorescence "Turn Off" chemosensors (L1-L4) for detection of Ni²⁺ in aqueous media are reported. The receptors (L1-L4) showed a distinct color change from yellow to red by addition of Ni²⁺ with spectral changes in bands at 535–550 nm. The changes are reversible and pH independent. The detection limits for Ni²⁺ by (L1-L4) are in the range of 0.2–0.5 µM by UV–Visible data and 0.040–0.47 µM by fluorescence data, which is lower than the permissible value of Ni²⁺ (1.2 µM) in drinking water defined by EPA. The binding stoichiometries of L1-L4 for Ni²⁺ were found to be 2:1 through Job's plot and ESI–MS analysis. Moreover the receptors can be used to quantify Ni²⁺ in real water samples. Formation of test strips by the dip-stick method increases the practical applicability of the Ni²⁺ test for "in-the-field" measurements. DFT calculations and AIM analyses supported the experimentally determined 2:1 stoichiometries of complexation. TD-DFT calculations were performed which showed slightly decreased FMO energy gaps due to ligand–metal charge transfer (LMCT).

The development and synthesis of chemosensors for selective and sensitive detection of heavy and transition metal ions is an active area of present day research due to their substantial effects on the environment and biological systems[1–3]. The sensing of metal ions in aqueous media is a complex task due to the presence of competitive interactions between the solvent and guest for receptor binding sites[4,5]. Among the various transition metals, nickel is an important element due to its widespread use in industry (Ni–Cd batteries), in ceramics and magnetic components for computers, metallurgical processes (electroplating), rods for arc welding, surgical and dental prostheses, and pigments for paints[6–8]. Nickel has a significant role in various enzymatic activities such as acireductone dioxygenases, carbon monoxide dehydrogenases, and catalysts for hydrogenation. It is also used as an essential trace element in biological systems, with significance in the biosynthesis and metabolism of some plants and microorganisms. However it is a toxic metal from a bio-medical point of view, as it can be easily absorbed by organs such as spleen liver, kidney etc. and may cause lung cancer, nasopharyngeal carcinoma, asthma, pneumonitis, and disorders of the central nervous system in humans. Deficiency or excessive levels of nickel also affect the life of many prokaryotic and eukaryotic organisms[9–13].

Considering all these facts, the selective monitoring of nickel is very important in environmental, biological and industrial samples. Various analytical methods such as flame atomic absorption spectrometry-electro thermal atomization (FAS-ETA), atomic absorption spectrometry (AAS), and inductively coupled plasma atomic emission spectrometry (ICP-AES) are widely used for detection of metal ions[14–19]. However, most of the methods need trained operators, sophisticated equipment and tedious sample preparation procedures, so there is still a need for simple, efficient and cost-effective methods for the micro level detection of heavy metals ions.

In recent years colorimetric, ratiometric, potentiometric and fluorescence sensors have gained attention for the selective detection of metal ions such as Ni²⁺ in biological and environmental samples. Colorimetric chemosensors show a distinct visible color change on selectively binding with a specific analyte without the use of expensive equipment, while the fluorescent sensors show fast responses towards analytes through fluorescence quenching or enhancement. These sensors have some drawbacks like poor solubility of probe, lack of selectivity, low sensitivity, and serious interference by other metals[20].

[1]Institute of Chemical Sciences, Bahauddin Zakariya University, Multan, Pakistan. [2]Department of Chemistry, Khwaja Fareed University of Engineering and Information Technology, Rahim Yar Khan 64200, Pakistan. [3]School of Chemistry, University of Bristol, Cantock's Close, Bristol BS8 1TS, UK. [4]Department of Botany and Microbiology, College of Science, King Saud University, P.O. 2455, Riyadh 11451, Saudi Arabia. ✉email: muhammad.khalid@kfueit.edu.pk; zahidshafiq@bzu.edu.pk
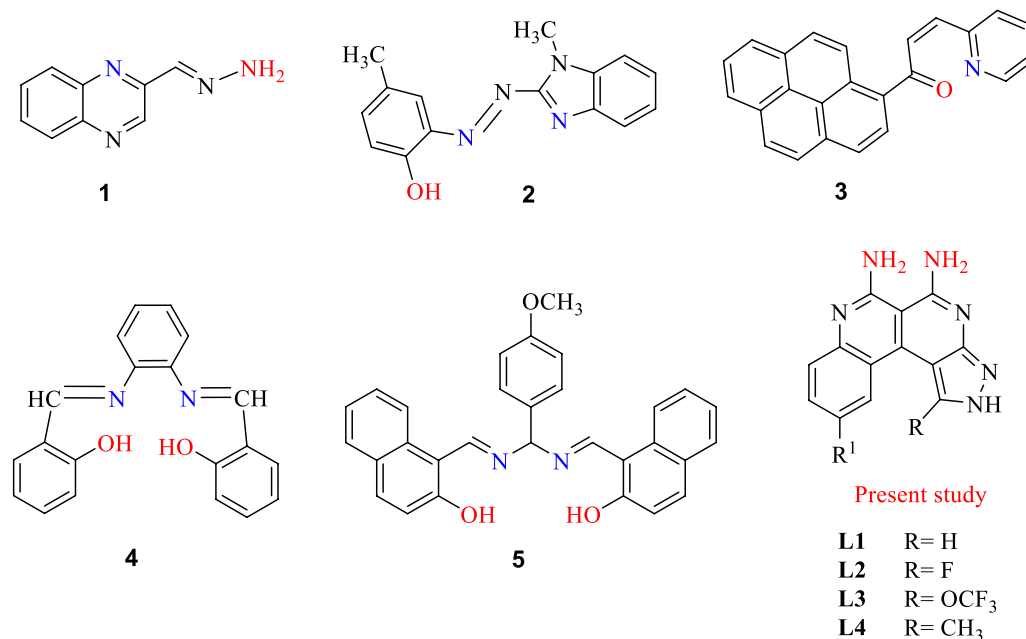
Figure 1. Some structural motifs employed in Nickel sensors, and L1-L4 from the present study.

Colorimetric sensors seem to be especially promising due to low cost, rapid detection and ease of use when compared to classical techniques as well as fluorescent sensors. Several organic molecules have been reported which showed colorimetric and fluorescent sensing of Ni^{2+} but few were capable of parts per million level detection. The signals from absorption and emission changes of light by chromophores or fluorophores provide information about the mechanism of sensing of metal cation (Ni^{2+}) by electron transfer (ET), charge transfer (CT), photoinduced electron transfer (PET), excited state intramolecular proton transfer (ESIPT) mechanism[21,22]. In recent times, the Goswami group reported a quinoxaline **1** based ratiometric chemosensor for the naked eye detection of Ni^{2+} in CH_3CN media[23]. Sarkar et al. developed benzimidazole based **2** as a ratiometric and colorimetric chemosensor for Ni^{2+} in DMSO[24]. Prabhu and co-workers developed a selective fluorescent turn on chemosensor for Ni^{2+} based on pyrene-conjugated pyridine[13] **3**. Biswajit Chowdhury et al. developed a Salen type Schiff base **4** colorimetric chemosensor with fluorescent enhancement for Ni^{2+}[25]. S. Santhi et al. developed the phenylmethanediamine based **5** as a colorimetric and turn off fluorescent sensor for detection of Co^{2+}, Ni^{2+} and Cu^{2+} in aqueous methanol solution[26] (Fig. 1).

Benzo[*c*]pyrazolo[2,7]naphthyridines and its derivatives have gained much attention in last few decades because they are biologically active alkaloids isolated from marine organisms such as perlolidine[27] (cellulose digestive inhibitor), subarine[28] (anti-HIV activity), meridine[29] (cytotoxic activity), amphimedine[30,31] (top isomerase II) inhibitor) and PDK-1 inhibitors[32].

In continuation of our research work in the field of molecular recognition, we herein report benzo[*c*]pyrazolo[2,7]naphthyridine-5,6-diamine based efficient colorimetric and/or *fluorescence off* sensors that can detect Ni^{2+} with sensitivity and selectivity in aqueous solutions. Many researchers have utilized amino group containing sensors like diaminonaphthalene[33], 1,8-naphthyridine-amine[34], 1,8-naphthyride-2-acetoamide[35], diaminophenazine and 1,2-diaminoanthracene-dione[36] to sense different metal ions like Cu^{2+}, Hg^{2+}, Fe^{3+}, Al^{3+}. Here we report sensors in which vicinal amino groups are placed on the benzo[*c*]pyrazolo[2,7]naphthyridine skeleton. Diamines L1-L4 serve as sensors for Ni^{2+} in aqueous solutions, utilizing the two amino groups as binding sites for the metal ion. The receptors detect the cation Ni^{2+} by both Chelation Enhanced Fluorescence Quenching (CHEFQ and an instant change in color from yellow to red. The chemosensors L1-L4 could be used as practical sensors for quantitative determination of nickel at ppm level in real water samples and also used in test kits to observe the color changes for Ni^{2+} by a dip stick method. Importantly the sensing potential of these derivatives can be tuned by the nature of the substituents R, i.e. electron donating (CH_3) and electron attracting (F, OCF_3), which affect the sensing properties. Quantum chemical computations (DFT) were performed to get detailed insight on the interaction between L4 and Ni^{2+} and are in good agreement with experimental findings.

Results and discussion

The benzo[c]pyrazolo[2,7]naphthyridine based chemosensors were synthesized as shown in Scheme S1. The isatins **6** react with malononitrile **7** via Knoevenogel condensation to form arylidenes. The formed arylidenes are then reacted with 3-amino-5-methylpyrazole **8** to synthesize spiro-intermediates which then undergo basic hydrolysis, cyclization, decarboxylation and aromatization to form target naphthyridine receptors (L1–L4)[37].
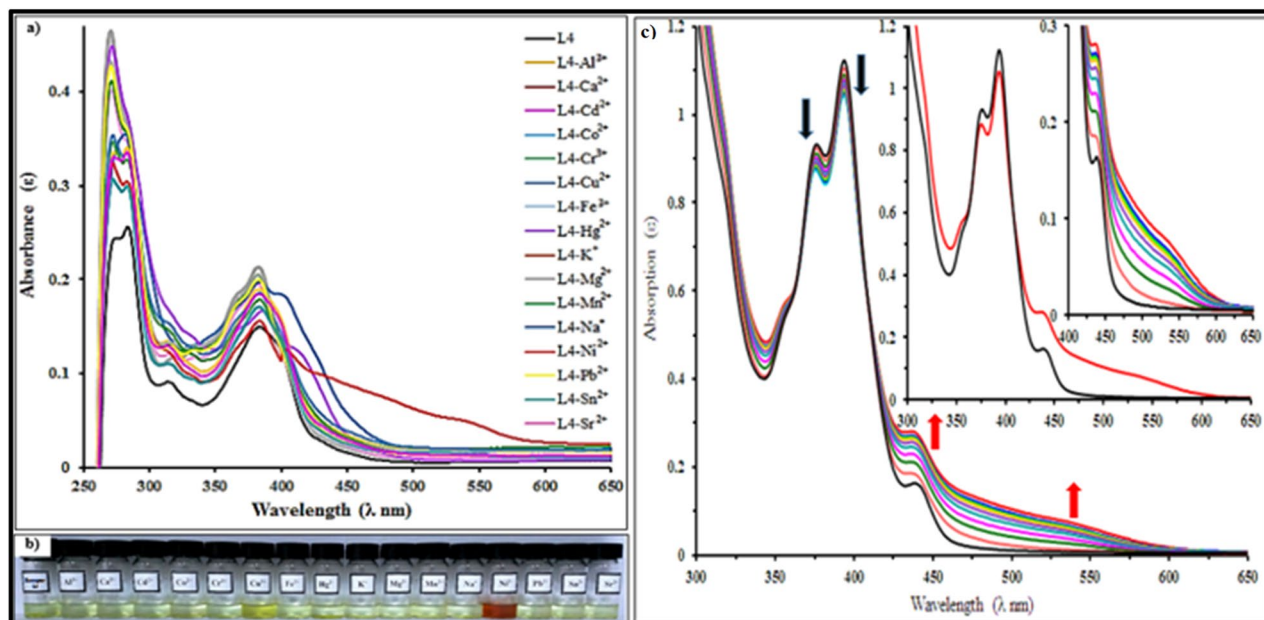
Figure 2. (**a**) Absorption spectral changes of L4 (20 μM) in the presence of different metal ions in DMSO–H$_2$O (v/v 1:2, HEPES buffer pH = 7.4), (**b**) Visual colorimetric response of receptor L4 upon addition of one equivalent various metal ions, (**c**) Absorbance titration spectra of receptor L4 (20 μM) in the presence of various concentrations of Ni^{2+} (0–12 μM) in DMSO–H$_2$O (v/v 1:2, HEPES buffer, pH = 7.4).

Receptor	UV–visible spectral band (nm)	Nickel addition (nm)
L1	273, 283, 398, 440	535
L2	274, 286, 384, 443	538
L3	261, 287, 380, 450	550
L4	273, 285, 396, 438	537

Table 1. UV–visible spectral bands of receptor L1-L4 with addition of nickel (II).

Spectrophotometric studies of L1–L4.

UV–visible study. Ligands L1–L4 were investigated as chemosensors for various metal ions (Al^{3+}, Ca^{2+}, Cd^{2+}, Co^{2+}, Cr^{3+}, Cu^{2+}, Fe^{3+}, Hg^{2+}, K$^+$, Mg^{2+}, Mn^{2+}, Na$^+$, Ni^{2+}, Pb^{2+}, Sr^{2+} and Sn^{2+}) by UV–visible spectroscopy. The preliminary colorimetric experiments involved addition of one equivalent of metal ions (1 × 10^{-3} M) to solutions of L1–L4 (1 × 10^{-3} M) in DMSO–H$_2$O (v/v 1:2), HEPES buffer of pH = 7.4 at room temperature. The addition of Ni^{2+} resulted in distinct visual color changes from yellow to red, but no color change was observed for other metal ions (Al^{3+}, Ca^{2+}, Cd^{2+}, Co^{2+}, Cr^{3+}, Cu^{2+}, Fe^{3+}, Hg^{2+}, K$^+$, Mg^{2+}, Mn^{2+}, Na$^+$, Pb^{2+}, Sr^{2+} and Sn^{2+}) Fig. 2a-b.

The binding interaction of L1–L4 with different metal ions was further monitored by investigating UV–visible absorption spectral changes as indicated in Table 1.

The UV–visible spectra of model receptor L4 showed a remarkable bathochromic shift in absorption spectrum at 537 nm which is in good agreement with the color change. This may possibly be ascribed to fast metal–ligand binding kinetics and the high thermodynamic affinity of Ni^{2+} for N-donor ligands[38]. The other examined metal ions did not cause any distinct spectral changes in the UV–visible spectrum at 537 nm under identical conditions. A similar pattern of absorption spectral changes were observed for L1-L3 (Figs. S1–S3).

The coordination between receptor L4 and Ni^{2+} was further demonstrated by UV–visible absorption spectral titrations involving sequential addition of Ni^{2+} aliquots (0–12 μM) to L4 (20 μM). It was observed that the intensity of the absorption bands at 537 nm and 438 nm increased while the absorption bands at 396 nm and 376 nm began to decrease until reaching limiting values. Moreover the emergence of isosbestic points at 365 nm and 410 nm during spectral titrations indicated the formation of stable complexes with definite stoichiometric ratios between L4 and Ni^{2+} [23] (Fig. 2c). Similar coordination behavior was observed for L1-L3 (Figs. S4–S6). These results suggest that receptors L1-L4 could be employed as colorimetric and ratiometric sensors for Ni^{2+} and discriminating against different transition metal ions (Fe^{3+}, Cu^{2+}, Co^{2+}, Pb^{2+}, Hg^{2+}) which are normally difficult to differentiate.

Fluorescence study. Photophysical complexation studies of L1-L4 at room temperature with metal ions were also performed with fluorescence spectroscopy. The fluorescence spectra of L4 showed an emission band at 470 nm (λ_{ex} = 390 nm) in DMSO–H$_2$O (v/v 1:2, HEPES buffer, pH = 7.4). Amongst addition of different metal
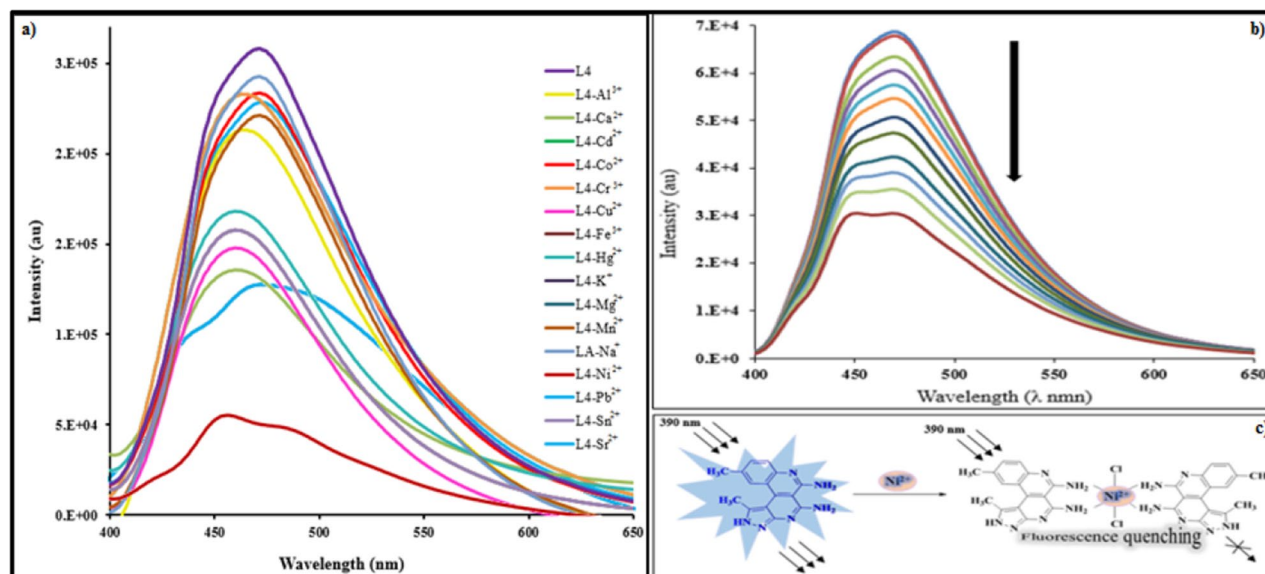
Figure 3. (**a**) Fluorescence spectral changes of L4 (20 μM) in the presence of different metal ions in DMSO–H₂O (v/v 1:2, HEPES buffer pH = 7.4), (λ_{ex} = 390 nm), (**b**) Fluorescence spectra of receptor L4 (20 μM) in the presence of various concentrations of Ni²⁺ (0–12 μM) HEPES buffer, pH = 7.4 (λex = 390 nm), (**c**) Proposed detection mechanism of receptor L4 to Ni²⁺.

ions (Al^{3+}, Ca^{2+}, Cd^{2+}, Co^{2+}, Cr^{3+}, Cu^{2+}, Fe^{3+}, Hg^{2+}, K^+, Mg^{2+}, Mn^{2+}, Na^+, Ni^{2+}, Pb^{2+}, Sr^{2+} and Sn^{2+}), the emission band at 470 nm underwent significant quenching with Ni²⁺ in comparison with the other metal ions (Fig. 3a). Similar patterns of fluorescence spectral changes were observed for L1-L3 (Figs. S7–S9).

The coordination behavior of L4 was examined via fluorescence titrations at room temperature. The sequential addition of Ni²⁺ (0–12 μM) to receptor L4 caused a substantial decrease of emission intensity at 470 nm, indicating "*turn-off*" behavior of the receptor (Fig. 3b). The rigid and planar structure of L4 molecule makes it a highly fluorescent compound. However when chelation occurs between the NH_2 groups of receptor L4 and Ni²⁺, the amino groups lose their ability to donate electron density into the fluorophore due to ligand–metal charge transfer (LMCT) which causes the Chelation Enhancement Quenching Effect (CHEQ) and quenching of emission potential[39] (Fig. 3c). Similar coordination behavior was observed for L1-L3 (Figs. S10–S12).

Binding stoichiometry, association constant and detection limit. The binding stoichiometry of the complexes were further explored by Job's continuous variation method[40] by plotting mole fraction versus changes in absorption intensity at 535 nm for L1, 538 nm for L2, 550 nm for L3 and 537 nm for L4, respectively. The Job's plots (Fig. S13) indicate maximum values at 0.7 corresponding to the formation of complexes with 2:1 stoichiometry between L1–L4 and Ni²⁺.

The association constants K_a of receptors L1–L4 with Ni²⁺ were determined by analysis of the UV–visible and fluorescence data using the Benesi–Hildebrand equation[41]

$$\frac{1}{(A - A_o)} = \frac{1}{\left\{(A_{max} - A_o)K_a[Ni^{2+}]^n\right\}} + \frac{1}{(A_{max} - A_o)}$$

(Figure S14, S15) and are listed in Table S1.

The association constant values are in range of those 10^3–10^6 reported for Ni²⁺ sensing chemosensors[42]. The trend of K_a values shows that L4-Ni²⁺ complex is stronger than the other receptor complexes. Moreover the association constants obtained by UV–visible data were on the same order of trend for as those obtained from fluorescence data i.e. L4-Ni²⁺ > L3-Ni²⁺ > L2-Ni²⁺ > L1-Ni²⁺.

The detection limits of L1–L4 for Ni²⁺ as colorimetric sensors were determined by naked eye, absorption and fluorescence spectral changes Table 2.

For naked eye detection, the receptor L4 showed a distinct color change at a minimum concentration of 1×10^{-6} M for Ni²⁺ (Fig. 4/S16). Moreover, the detection limits determined by absorption and fluorescence spectral changes on the basis of $3S_B/S$ [43] for L4 and Ni²⁺ were found to be 2.43×10^{-7} M and 4.03×10^{-8} M respectively. These values are lower than EPA drinking water guidelines (1.2×10^{-6} M for Ni²⁺ [44]) and revealed that L4 is highly efficient in sensing Ni²⁺ even at minute levels.

Proposed sensing mechanism. *ESI–MS, IR and ¹HNMR titrations.* The coordination mechanism of L4 to Ni²⁺ was explored by ESI–MS and IR titration experiments. The ESI mass spectra of L4 showed a peak at m/z: 279.17 [M + H]⁺ corresponding to [L4 + H]⁺. After titration of L4 with Ni²⁺ a signal at *m/z*: 685.58 for [2L4 + Ni + Cl₂ + H]⁺ (calculated *m/z* = 684) indicated the formation of a 2:1 stoichiometry complex between L4 and Ni²⁺ (Fig. S17).

| Receptor | Detection limit ($3S_B/S$) M | | Detection limit (Naked eye) M |
	Absorbance	Emission	
L1	5.62×10^{-7}	4.76×10^{-7}	1×10^{-5}
2	5.56×10^{-7}	1.19×10^{-7}	1×10^{-5}
L3	3.88×10^{-7}	6.61×10^{-8}	1×10^{-5}
L4	2.43×10^{-7}	4.03×10^{-8}	1×10^{-6}

Table 2. Detection limit of receptor L1-L4 with nickel.

Figure 4. Naked eye detection limit for receptor L4.
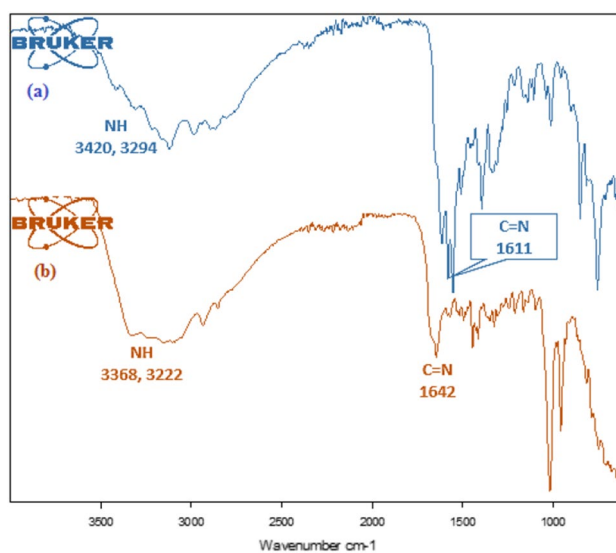
Figure 5. IR spectra of (**a**) receptor L4 and (**b**) receptor L4–Ni^{2+} complex.

FT-IR titrations were performed by using a Bruker Alpha FT-IR. Figure 5 shows a comparison of the IR spectra of L4 before and after the addition of Ni^{2+}. The sharp peaks present at 3420, 3294 and 3109 cm^{-1} due to NH stretching frequencies in free receptor L4 were broadened by adding Ni^{2+}, suggesting the involvement of NH$_2$ group in coordination with Ni^{2+} to form complex[45,46]. To further investigate the interaction behavior between L4 and Ni^{2+}, we carried out ^{1}HNMR titrations but these were not successful due to paramagnetic property of L4-Ni^{2+} complex[42]. The plausible sensing mechanism of L4 for Ni^{2+} is shown in Scheme 1.

Metal ion selectivity.   An important feature of receptor L4 is its selectivity towards analytes. This was examined by competitive titration experiments (Fig. 6a). The intensity of the absorption band at 537 nm due to complex formation of L4-Ni^{2+} is not disturbed at all in the presence of other metal ions (Al^{3+}, Ca^{2+}, Cd^{2+}, Co^{2+}, Cr^{3+}, Cu^{2+}, Fe^{3+}, Hg^{2+}, K$^+$, Mg^{2+}, Mn^{2+}, Na$^+$, Pb^{2+}, Sr^{2+} and Sn^{2+}). Thus the receptor L4 shows excellent binding affinity for Ni^{2+}, which should hold in physiological samples where Cu^{2+}, Co^{2+}, Fe^{3+}, Hg^{2+} and Pb^{2+} usually coexist with analyte. This distinct selectivity for Ni^{2+} may be due to matching of the geometry of the receptor with the ionic radius of Ni^{2+} [13].

The UV–visible absorption spectra of the L4-Ni^{2+} complex with various anions was recorded to check the stability of complex. No change in the absorption band at 537 nm was observed (Fig. 6b-c). This clearly indicates that the stability of the complex is unaffected by the presence of various anions.
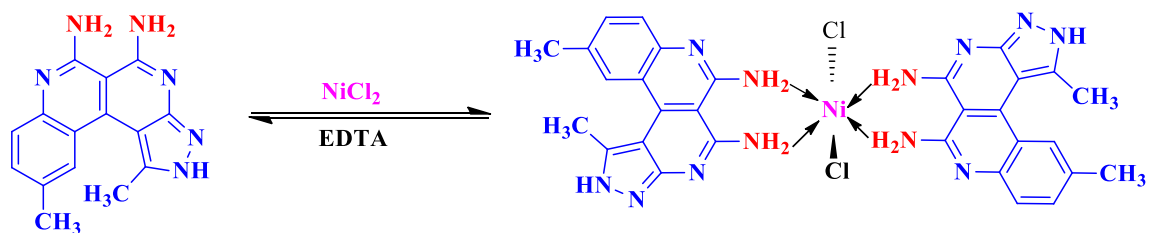
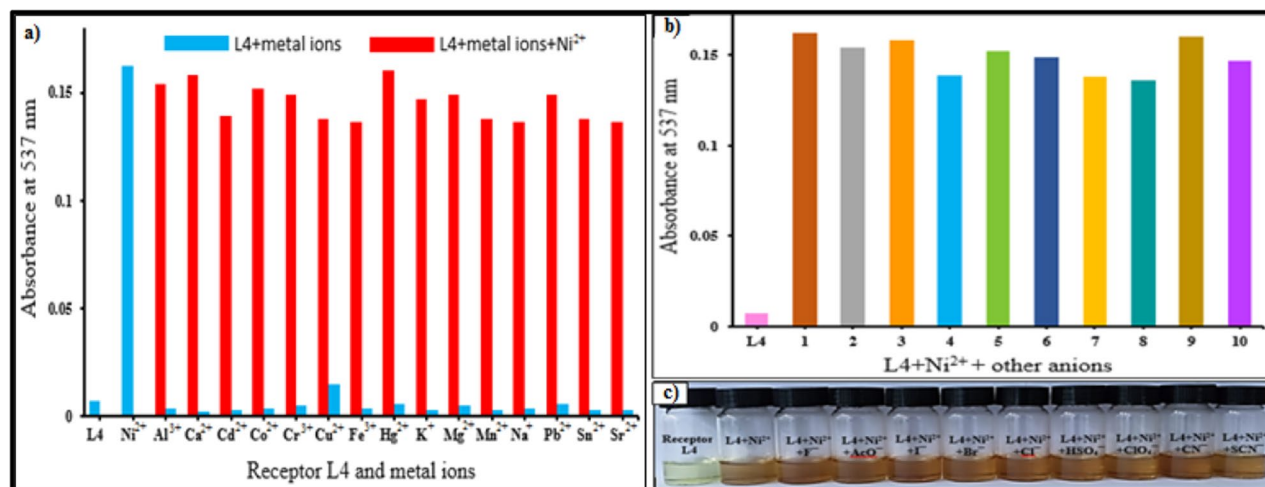**Scheme 1.** The plausible sensing mechanism of Ni²⁺ and with L4.

Figure 6. (**a**) Absorbance responses of L4 (20 µM) in the presence of Ni²⁺ (10 µM) with 10 equivalents of various metal ions in DMSO–H₂O (v/v = 1:2) HEPES buffer solutions at pH = 7.4, (**b**) Absorbance at 537 nm of receptor L4 (20 µM) in the presence of Ni²⁺ (10 µM) in the presence of 10 equivalents of various anions in DMSO–H₂O (v/v = 1:2) HEPES buffer solutions at pH = 7.4, (**c**) The color changes of L4 upon addition of Ni²⁺ and various anions (1–10).

pH effect study. In order to investigate the effect of pH on the absorption response of receptor L4 to Ni²⁺, a series of solutions with pH values ranging from (2.0 – 12.0) were prepared (Fig. S18).

At pH 2.0–3.0, the receptor L4 shows no substantial response to Ni²⁺ in absorption spectroscopy. The absorption of the L4-Ni complex at 537 nm is maximum and constant in pH range 7.0 – 8.0. Above pH 8.0, absorbance decreased gradually. The results suggest that biological and environmental applications at physiological pH should be feasible. The color of L4– Ni²⁺ complex remained red between pH 4–11, which indicated that Ni²⁺ could be clearly detected over a wide range of pH 4–11.

Reversibility of receptor L4. The reversibility of receptor L4 towards Ni²⁺ was examined by adding ethylenediaminetetracetic acid (EDTA, 1 equiv.) to the complexed solution of L4 and Ni²⁺ (Fig. 7).

The solution's color changed from red to light yellow (original color of L4). Upon addition of Ni²⁺ again the absorbance at 537 nm was recorded. The absorption changes in spectral bands were reversible even after several cycles with alternative sequential addition of Ni²⁺ and EDTA. These results indicate that L4 could be recyclable as an *off–on-off* receptor by the interaction of EDTA with L4–Ni²⁺ (Scheme 1). Such regeneration and reversibility could be valuable for the fabrication of Ni²⁺ sensors.

Synthesis of the L4–Ni²⁺ complex. The Ni²⁺ complex of receptor L4 was synthesized by mixing an Ni²⁺ salt with L4 using 1:2 ratio in DMSO-H₂O solvent mixture. The yellow solution of the ligand immediately turned to red colored solution. The solution was further refluxed to get the solid product (Scheme 2).

Red solid, Yield: 84%, mp > 300 °C; λ_{max}: 535 nm; λ_{em}: 473 (λ_{ex} = 340); IR (ATR, cm⁻¹): 3368, 3222, (NH), 1642, 1541, 1438, 1339, 1238, 1110, 1031, 1002, 825, 731; MS (ESI) m/z: 685.41 [2L4 + Ni + Cl₂]⁺; Molar conductance: 0.41 S cm² M⁻¹; μ_{eff} (B.M.): 2.98.

The synthesized complex of L4–Ni²⁺ was characterized using UV–Visible, fluorescence spectroscopy, molar conductance, SEM, ESI–MS and magnetic moment analysis. A 10⁻³ M solution of the L4–Ni²⁺ complex exhibited a molar conductance value of 0.4 S cm² M⁻¹ which suggests non-electrolyte behavior in DMSO solution. The ESI–MS of the synthesized L4–Ni²⁺ complex (Fig. 8a) showed the molecular ion peak at m/z 685.41 which matched very well with the calculated molar mass of [2L4 + Ni + Cl₂ + H]. Furthermore, SEM analysis was carried out to obtain a better understanding of morphological difference before and after the addition of Ni²⁺ to L4 receptor (Fig. 8b-c). SEM images of receptor L4 show dense sprinkled elliptical shapes which are transformed into
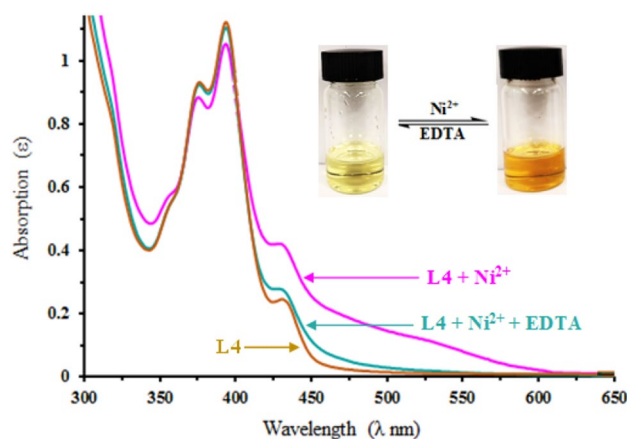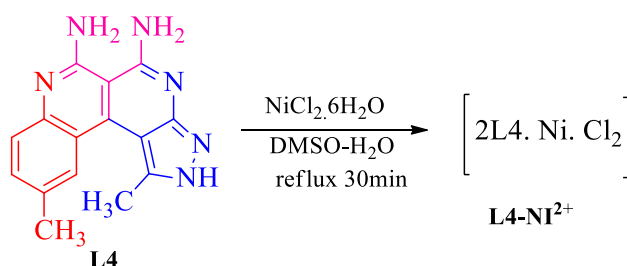
Figure 7. Changes in absorbance spectra of L4 (20 μM) in DMSO–H$_2$O solution (1:2 v/v, HEPES buffer, pH = 7.4) in the presence of Ni^{2+} and EDTA.

Scheme 2. Preparative route for L4-Ni^{2+} complex.

a rough stone like structure after complexation with Ni^{2+}. Magnetic studies were used to confirm the geometry of the synthesized metal complex L4–Ni^{2+}. The room temperature magnetic moment value of the solid complex is μ_{eff} (B.M.): 2.98 in line with an octahedral environment (2.9–3.3 B.M.) around the metal ion[47]. The proposed octahedral geometry is also supported by mass spectral analysis.

Practical application. In order to investigate the potential use of receptor L4 in real water samples, a calibration curve was drawn, which showed a good linear relationship (R2 = 0.9996, n = 3) between the absorbance of the L4–Ni^{2+} complex and the Ni^{2+} concentration (0–5 μM) at 537 nm (Fig. S19). The receptor L4 was used for the estimation of Ni^{2+} in drinking water, tap water and industrial waste water samples (Table 3). All water samples were analyzed in triplicate with good recoveries and RSD values. The results indicate that receptor L4 is highly specific and sensitive for Ni^{2+} estimations in environmental samples.

To explore another application of receptor L4, test kits were prepared by immersing filter paper in receptor L4 (1 × 10^{-3} M, HEPES buffer, pH = 7.4) and then air drying to investigate a "dip-stick" method for detection of Ni^{2+}. When the prepared test strips were immersed into aqueous solutions of Ni^{2+} with different concentrations, clear color changes from yellow to red were observed (Fig. 9). The results showed that discernible concentrations of Ni^{2+} can be as low as 1 × 10^{-5} M. The "dip-stick" method did not require any additional equipment for detection of Ni^{2+} and should be highy attractive for "in-the-field" measurements.

Theoretical details on structural aspects of L4–Ni^{2+}. *Computational details.* In order to evaluate the interaction between L4 and Ni^{2+} theoretical calculations on the L4-NiCl$_2$ complex were performed. Geometry optimization calculations were performed for the free species L4 and NiCl$_2$, and complexes L4-NiCl$_2$ and 2L4-Ni$_2$Cl$_2$ (with two L4 molecules). The calculations employed the DFT method by applying the M06L[48] functional and def2-SVP[49] basis set. The calculations were carried out with the Gaussian 09[50] package (Revision D.01). To evaluate the interactions in the complexes we performed Atoms in Molecules[51–53] (AIM) analysis. The AIM analyses were carried out with Multiwfn[54] package from single-point calculations with M06L functional and def2-TZVP basis set with SMD solvent model with DMSO as solvent and visualized with VMD[55]. Frontier Molecular Orbitals (FMO) analyses were performed to investigate the effect of L4 complexation with Ni^{2+}. The FMO analyses were carried out with TD-DFT single-point calculations (from their respective optimized geometries) by applying the M06-2X[56]/def2-TZVP[49] level of theory with the SMD solvent model and DMSO as solvent in the Orca[57] package.
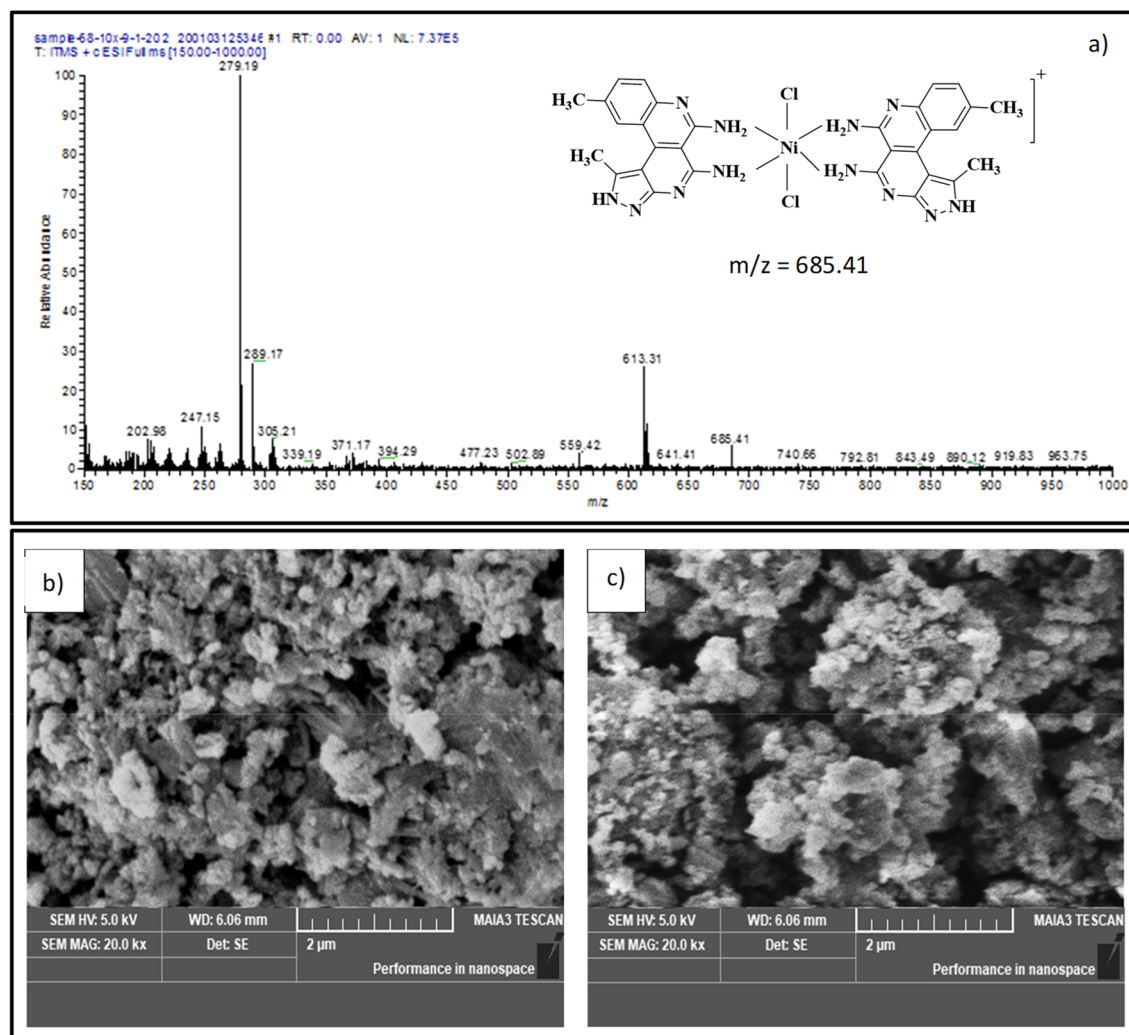
Figure 8. (**a**) ESIMS of L4-Ni^{2+} complex (**b**) The SEM images of Receptor L4 (**c**) L4-Ni^{2+} complex.

Sample	Ni^{2+} added (µM)	Ni^{2+} found (µM)	Recovery (%)	RSD (n = 3) %
Drinking water	0.00	0.00		
	0.50[a]	0.47[b] (0.50)[c]	94.0	2.13
	1.00[a]	0.98[b] (1.00)[c]	98.0	1.97
	2.00[a]	1.97[b] (2.00)[c]	98.5	1.21
Tap water	0.00	0.00		
	0.50[a]	0.46[b] (0.50)[c]	92.0	2.43
	1.00[a]	0.97[b] (1.00)[c]	97.0	2.04
	2.00[a]	1.96[b] (2.00)[c]	98.0	1.68
Industrial waste water	0.00	0.00		
	0.50[a]	0.45[b] (0.50)[c]	90.0	2.89
	1.00[a]	0.96[b] (0.99)[c]	96.0	3.04
	2.00[a]	1.95[b] (1.99)[c]	97.5	1.89

Table 3. Determination of Ni^{2+} in water samples. [a]Artificially spiked concentration of Ni^{2+}. [b]Results obtained by newly synthesized receptor L4. (·)[c]Results obtained from ICP-OES analysis.

Theoretical calculations. The experimental results indicated complex formation with 2:1 stoichiometry between L4 and NiCl$_2$. Thus, we performed calculations for free L4 and NiCl$_2$, for L4-NiCl$_2$ complexes (with one L4 molecule) and for 2L4-NiCl$_2$ complexes (with two L4 molecules) as shown in Fig. 10. The relative energies are shown in Table S2 and demonstrate that the complexation between L4 and NiCl$_2$ is spontaneous. The energies for complexation with one or two L4 molecules showed that the complex with two L4 molecules is more stable than with
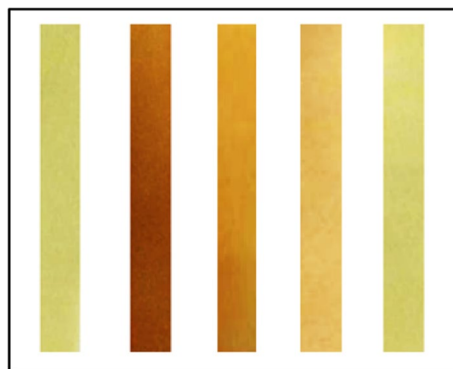
Figure 9. Color change of the test strips of L4 (1×10^{-3} M) at various concentrations of Ni^{2+} in water, from left to right: 0, 1×10^{-3} M, 1×10^{-4} M, 1×10^{-5} M and 1×10^{-6} M.

L4 + NiCl$_2$
ΔG = 0.00 kcal/mol

L4-NiCl$_2$
ΔG = -50.28 kcal/mol

2L4-NiCl$_2$
ΔG = -57.61 kcal/mol
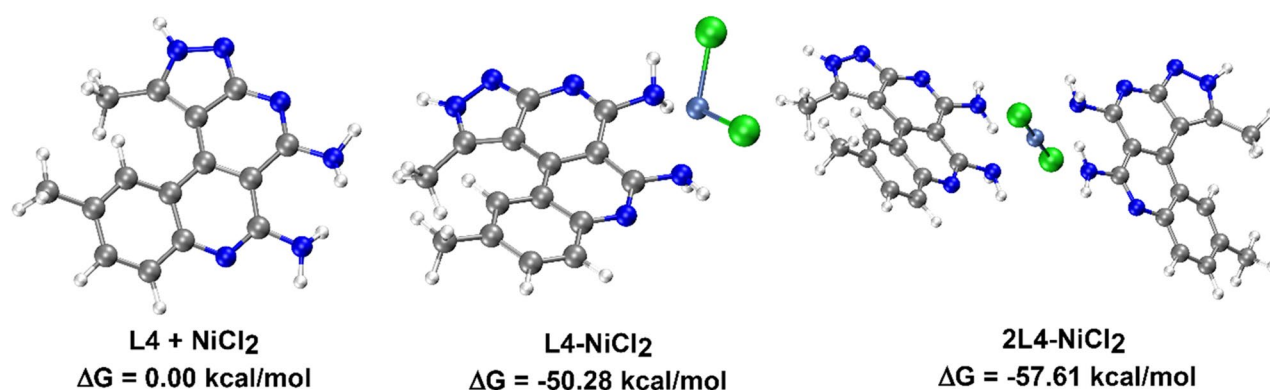
Figure 10. Scheme of optimized geometries (with M06L/def2-SVP method) for L4-NiCl$_2$ complexes and 2L4-NiCl$_2$ complexes with Ni^{2+} with their respective relative Gibb free energies.
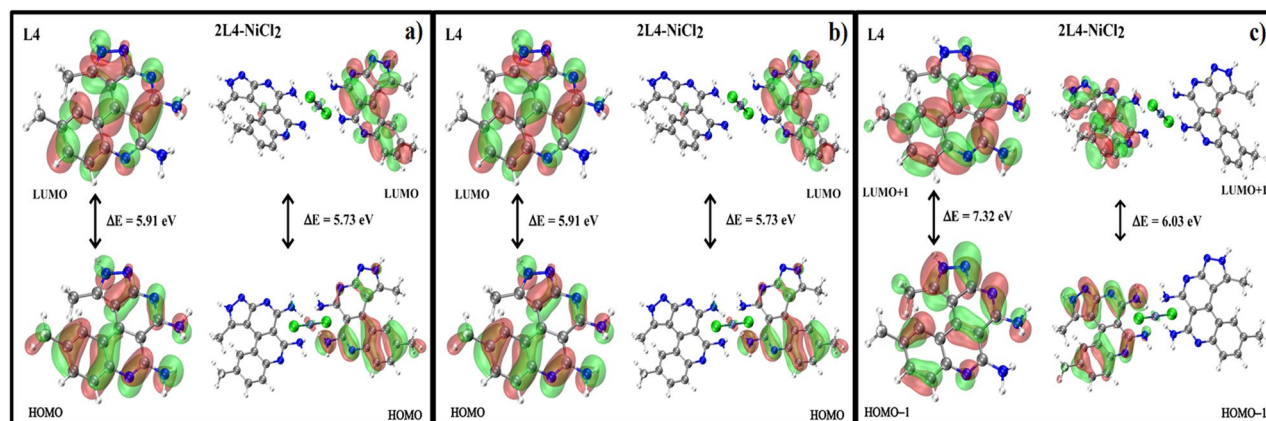

Figure 11. (**a**) FMO surfaces plot. HOMO and LUMO for L4 (left) and 2L4-NiCl$_2$ (right), (**b**) FMO surfaces plot. HOMO-1 and LUMO+1 for L4 (left) and 2L4-NiCl$_2$ (right), (**c**) FMO surfaces plot. HOMO-2 and LUMO+2 for L4 (left) and 2L4-NiCl$_2$ (right).

just one molecule in agreement with experimental results. Thus, the FMO and AIM analyses were performed just for complexes with two L4 molecules.

FMO and GRD analysis. The energies for frontier molecular orbitals of free L4 and the 2L4-NiCl$_2$ complex are shown in Table S3. It was verified through the FMO analysis species that the complexation between L4 and NiCl$_2$ causes a slight decrease of the frontier molecular orbitals and the 2L4-NiCl$_2$ complex showed lower HOMO/ LUMO energy gaps, particularly for HOMO-1/LUMO+1 and HOMO-2/LUMO+2 which are related to the interaction with nickel. The surfaces for frontier molecular orbitals of L4 and 2L4-NiCl$_2$ are shown in Fig. 11.
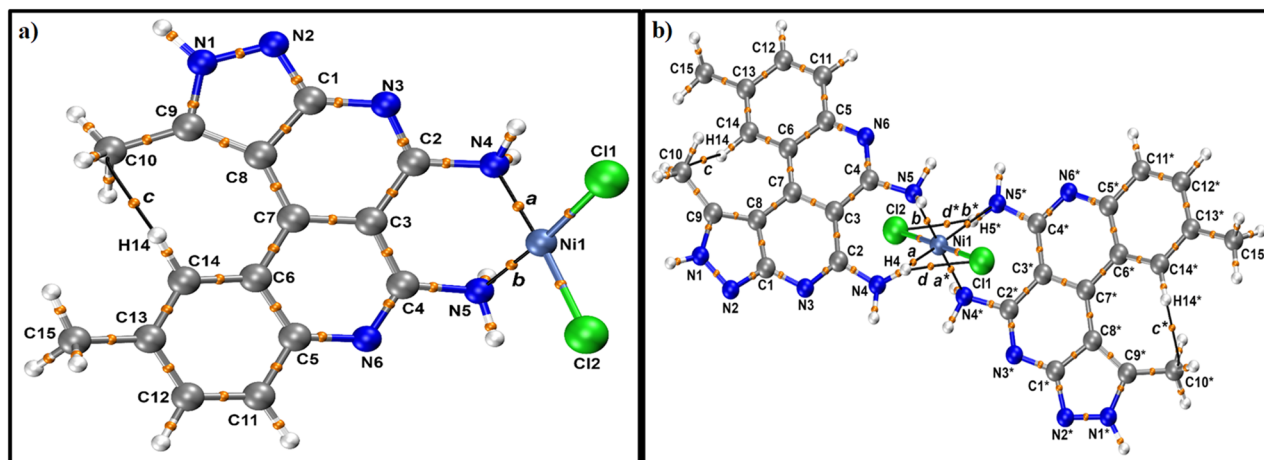
Figure 12. (**a**) AIM molecular graph for L4-NiCl$_2$. Bond Critical Points (orange spheres) and Bond Paths (solid dashed black lines), (**b**) AIM molecular graph for 2L4-NiCl$_2$ Bond Critical Points (orange spheres) and Bond Paths (solid dashed black lines).

AIM analysis. The AIM properties for the 2L4-NiCl$_2$ complexes are shown in the Table S4 and their respective molecular graphs are shown in Fig. 12a-b respectively. The characterization of strengthening of the interaction between L4 and NiCl$_2$ was performed through the topological analysis of the electronic density. Therefore, the presence of an interaction between atoms was featured by the presence of a Bond Path (BP) between two attractor (atoms in a molecule) and their characteristics such covalence and strength were determined though the AIM properties in their Bond Critical Points (BCPs). The main AIM properties that were evaluated in this work were the electronic density, $\rho(r)$, Laplacian of density, $\nabla^2\rho(r)$, and density of potential energy, $V(r)$.

Thus, the presence of the interaction between NH$_2$ and Ni was revealed by the presence of a BP between N and Ni atoms. The AIM molecular graphs with their respective labels are shown in Fig. 12a-b. The BCPs ***a*** and ***b*** are related to the Ni–N bonds in the complexes L4-NiCl$_2$ and 2L4-NiCl$_2$. The complexes' formation showed BCPs *a* and *b* with positive value of $\nabla^2\rho(r)$ with can indicate a non-covalent interaction or ionic bond. When the values of electronic density, $\rho(r)$, were analyzed for these BCPs was verified that the BCPs *a* for both complexes showed high negative values of density of potential energy, $V(r)$, which indicates that the bonds related to BCPs *a* have the characteristic of ionic bonds. The BCP b L4-NiCl$_2$ also showed an ionic characteristic. However, the 2L4-NiCl$_2$ complex showed the weakening of one of their Ni-NH$_2$ interaction to formation of another Ni-NH$_2$ interaction with the second L4 molecule. Thus, the 2L4-NiCl$_2$ showed two ionic bonds between N-Ni (BCPs *a* and *b**) with $\rho(r) = 0.0922$ a.u. and $\rho(r) = 0.0901$ a.u., respectively, and two non-covalent interactions between N-Ni (BCPs *b* and *a**), that were revealed by the presence of $\nabla^2\rho(r) > 0$, though, with low values of $\rho(r)$ ($\rho(r) = 0.0202$ a.u. and $\rho(r) = 0.0181$ a.u., respectively) and low negative values of $V(r)$. While the L4-NiCl$_2$ complex showed two ionic bonds with the same L4 with BCPs a and *b*, the 2L4-NiCl$_2$ complex showed two ionic bonds and several non-covalent interactions (BCPs *c*, *d*, *c** and *d**) between L4 and NiCl$_2$, Thus, such non-covalent interactions should be related with the stabilization of 2L4-NiCl$_2$ complex in relation to L4-NiCl$_2$. Beyond the interaction between N atoms from L4 and Ni^{2+} was verified the presence of NH···Cl interaction (BCPs *d* and *d** with $\rho(r) = 0.0165$ a.u. and $\rho(r) = 0.0133$, respectively) in the 2L4-NiCl$_2$ complex which should increase the NH stretching frequencies shift in relation to free L4 which agree with experimental results.

Conclusion

In summary, we have successfully characterized the photophysical properties of benzo[*c*]pyrazolo[2,7]naphthyridines (L1-L4) which were prepared by a green synthetic route. The receptors (L1-L4) allow selective and sensitive sensing of Ni^{2+} in aqueous media over a wide range of pH (4–11) even in the presence of competitive ions i.e. Fe^{3+}, Cu^{2+}, Co^{2+}. A unique colorimetric response to Ni^{2+} is observed (yellow to red) through coordination of receptor and Ni^{2+} complex could be recyclable through treatment with EDTA. The detection limit of Ni^{2+} was found to be in range of 0.2–0.5 μM for (L1-L4) by UV–Visible data, and 0.040–0.47 μM by fluorescence data, which is lower than the permissible value of Ni^{2+} (1.2 μM) in drinking water and opens a potential application of the receptors in recognizing Ni^{2+} in environment. The binding stoichiometries of (L1-L4) with Ni^{2+} were found to be 2:1 through Job's plot and ESI–MS analysis. The fluorescence properties of the receptors were evaluated with fluorescence quenching by coordination with Ni^{2+}. As a practical application, the most efficient receptor L4 could be used to quantify and detect Ni^{2+} in real water samples and also applied for fabrication of test kits using the "dip-stick" method. To the best of our knowledge, receptors (L1-L4) are the first reported multifunctional, naked eye chemosensors for sensing of Ni^{2+} in aqueous solutions. Theoretical calculations demonstrate that the stoichiometry of complexation between L4 and NiCl$_2$ should be 2:1 as experimentally verified. The non-covalent interactions between L4 and NiCl$_2$ in the formed complex, particularly involving the –NH$_2$ groups can broaden the NH stretching frequencies, which is consistent with the experimental results. The FMO demonstrate the complexation with Ni decreases the frontier molecular orbitals and their respective energy gaps.

Experimental

Materials and equipment.   All the solvents and reagents used for synthesis were of analytical grade and used as received. Infrared (IR) spectra were recorded by Bruker Alpha FT-IR spectrophotometer. Mass spectra were recorded by a Thermo Scientific LTQ-XL system fitted with electrospray ionization (ESI) source, Jeol 600 MS Route, and Jeol Hx110 mass spectrometer (EI-HR). Pre-coated aluminum sheets of silica gel 60 GF254 (Merck) were used as TLC plates to check the purity of compounds. Quantitative determination of nickel was carried out by Inductively Coupled Plasma-Optical Emission Spectrometer (iCAP6500 ICP-OES, Thermo Scientific, Cambridge, United Kingdom). The pH was measured using a Metrohm, 78 l pH/ion meter. Magnetic moments were estimated using a magnetic susceptibility balance (Sherwood Auto, 2005) at room temperature. Metal conductance of metal complexes was recorded by using an InoLab IDS Multi9430 conductivity meter.

Synthesis of receptors (L1–L4).   The synthesis of receptors (L1–L4) was carried out in two steps following our previously reported protocol[37].

Synthesis of L4-Ni^{2+} complex.   The DMSO (3 ml) solution of L4 (0.2 mmol) and 2 ml water solution of NiCl$_2$.6H$_2$O (0.12 mmol) were mixed and stirred at room temperature for 30 min. The yellow solution of receptor L4 immediately turned to red colored solid product, which was filtered and washed with distilled water.

UV–visible and fluorescence titrations.   Stock solutions of receptors, L1–L4 (1×10^{-3} M) were prepared in DMSO–H$_2$O (v/v = 1:2) using HEPES buffer solution (pH = 7.4). Stock solutions of different guest metal ions (1×10^{-3} M) were prepared by using chloride salts of the respective metals (Al^{3+}, Ca^{2+}, Cd^{2+}, Co^{2+}, Cr^{3+}, Cu^{2+}, Fe^{3+}, Hg^{2+}, K$^+$, Mg^{2+}, Mn^{2+}, Na$^+$, Ni^{2+}, Pb^{2+}, Sr^{2+} and Sn^{2+}) and the stock solutions (1×10^{-4} M) of different anions like Cl$^-$, I$^-$, Br$^-$, CN$^-$, ClO$_4^-$, F$^-$, HSO$_4^-$, AcO$^-$ and SCN$^-$ from TBA salts were prepared in deionized water. For ratiometric titrations, the solutions of various concentrations of receptor with increasing concentration of cations were prepared separately.

Competition experiments.   For Ni^{2+} the stock solution of receptor L4 (1×10^{-3} M) was prepared in DMSO–H$_2$O (v/v 1:2) using HEPES buffer of pH = 7.4. Stock solution of different guest cations (1×10^{-3} M) were prepared in water and added to 4 mL of the solution of receptor L4 to give 10 equivalents of metal ions. Then Ni^{2+} solution was added into mixed solutions of each metal ion to make 1 equivalent. A few minutes after mixing, the UV–visible spectra were recorded at room temperature.

Water sample collection and Ni^{2+} determination.   The drinking water samples, tap water and industrial waste water samples were collected, preserved and stored in plastic containers for Ni^{2+} analysis. Industrial waste water samples were filtered prior to analysis. Each sample was analyzed in triplicate using receptor L4 and ICP-OES as standard method (Table 3). Spiking and recovery method was used in order to validate chemosensing performance of our newly developed sensor L4. UV–visible spectral measurement of water samples containing Ni^{2+} was carried out by adding 0.5 mL of receptor L4 to 2.5 mL of sample solutions and pH of solution was maintained at 7.4 using HEPES buffer. The solutions were allowed to stand for 10 min at room temperature and absorption measurements were taken at 537 nm. Filtered water samples were directly used for ICP-OES analysis.

Colorimetric test strips.   The test kits were prepared by immersing filter paper strips in to receptor L4 solution 1×10^{-3} M (DMSO–H$_2$O (v/v 1:2) using HEPES buffer of pH = 7.4) and then dried in air. Then the pure water solution with different Ni^{2+} concentrations were prepared and the prepared test strips were immersed in water samples and color change from yellow to red was observed.

Magnetic moments.   Magnetic moments of the prepared solid complex were estimated by magnetic susceptibility balance Sherwood (Auto, 2005) at room temperature.

References
 1. Mulrooney, S. B. & Hausinger, R. P. Nickel uptake and utilization by microorganisms. *FEMS Microbiol. Rev.* **27**, 239–261 (2003).
 2. Ragsdale, S. W. Nickel-based enzyme systems. *J. Biol. Chem.* **284**, 18571–18575 (2009).
 3. Maier, R. (Portland Press Ltd., 2005).
 4. Singh, A., Singh, A. & Singh, N. A Cu (II) complex of an imidazolium-based ionic liquid: Synthesis, X-ray structure and application in the selective electrochemical sensing of guanine. *Dalton Trans.* **43**, 16283–16288 (2014).
 5. Raj, P. *et al.* Fluorescent chemosensors for selective and sensitive detection of phosmet/chlorpyrifos with octahedral Ni^{2+} complexes. *Inorg. Chem.* **55**, 4874–4883 (2016).
 6. Ragsdale, S. W. Nickel and Its Surprising Impact in Nature. Metal Ions in Life Sciences, Vol. 2. Edited by Astrid Sigel, Helmut Sigel, and Roland K. 14O. Sigel. (2008).
 7. Kasprzak, K. S., Sunderman, F. W. Jr. & Salnikow, K. Nickel carcinogenesis. *Mutation Research/Fundamental and Molecular Mechanisms of Mutagenesis* **533**, 67–97 (2003).
 8. Kuck, P. Nickel. United States Geological Survey, Mineral Commodity Summaries, January 2006. *United States Geological Survey*, 116–117 (2006).

9. Zambelli, B., Musiani, F., Benini, S. & Ciurli, S. Chemistry of Ni^{2+} in urease: Sensing, trafficking, and catalysis. *Acc. Chem. Res.* **44**, 520–530 (2011).
10. Staton, I. *et al.* Dermal nickel exposure associated with coin handling and in various occupational settings: assessment using a newly developed finger immersion method. *Br. J. Dermatol.* **154**, 658–664 (2006).
11. Stangl, G. I., Eidelsburger, U. & Kirchgessner, M. Nickel deficiency alters nickel flux in rat everted intestinal sacs. *Biol. Trace Elem. Res.* **61**, 253 (1998).
12. Heim, K. E. & McKean, B. A. Children's clothing fasteners as a potential source of exposure to releasable nickel ions. *Contact Dermatitis* **60**, 100–105 (2009).
13. Prabhu, J. *et al.* A simple chalcone based ratiometric chemosensor for sensitive and selective detection of Nickel ion and its imaging in live cells. *Sens. Actuators, B Chem.* **238**, 306–317 (2017).
14. Ohta, K., Ishida, K., Itoh, S.-I., Kaneco, S. & Mizuno, T. Determination of nickel in water by electrothermal atomic absorption spectrometry with preconcentration on a tungsten foil. *Microchim. Acta* **129**, 127–132 (1998).
15. Sarre, S., Van Belle, K., Smolders, I., Krieken, G. & Michotte, Y. The use of microdialysis for the determination of plasma protein binding of drugs. *J. Pharm. Biomed. Anal.* **10**, 735–739 (1992).
16. Mazloum, M., Niassary, M. S. & Amini, M. K. Pentacyclooctaaza as a neutral carrier in coated-wire ion-selective electrode for nickel (II). *Sens. Actuators B Chem.* **82**, 259–264 (2002).
17. Jankowski, K., Yao, J., Kasiura, K., Jackowska, A. & Sieradzka, A. Multielement determination of heavy metals in water samples by continuous powder introduction microwave-induced plasma atomic emission spectrometry after preconcentration on activated carbon. *Spectrochim. Acta Part B* **60**, 369–375 (2005).
18. Zendelovska, D., Pavlovska, G., Cundeva, K. & Stafilov, T. Electrothermal atomic absorption spectrometric determination of cobalt, copper, lead and nickel traces in aragonite following flotation and extraction separation. *Talanta* **54**, 139–146 (2001).
19. Sunil, A. & Rao, S. J. First derivative spectrophotometric determination of copper (II) and nickel (II) simultaneously using 1-(2-hydroxyphenyl) thiourea. *J. Anal. Chem.* **70**, 154–158 (2015).
20. Das, M. & Sarkar, M. Bis-pyridyl diimines as selective and ratiometric chemosensor for Ni (II) and Cd (II) metal ions. *ChemistrySelect* **4**, 681–692 (2019).
21 Chakraborty, S. & Rayalu, S. Detection of nickel by chemo and fluoro sensing technologies. *Spectrochim. Acta Part A: Mol. Biomol. Spectrosc.* **245**, 118915 (2020).
22. Biswas, S., Acharyya, S., Sarkar, D., Gharami, S. & Mondal, T. K. Novel pyridyl based azo-derivative for the selective and colorimetric detection of nickel (II). *Spectrochim. Acta Part A Mol. Biomol. Spectrosc.* **159**, 157–162 (2016).
23. Goswami, S. *et al.* A highly selective ratiometric chemosensor for Ni 2+ in a quinoxaline matrix. *New J. Chem.* **38**, 6230–6235 (2014).
24. Sarkar, D., Pramanik, A. K. & Mondal, T. K. Benzimidazole based ratiometric and colourimetric chemosensor for Ni (II). *Spectrochim. Acta Part A Mol. Biomol. Spectrosc.* **153**, 397–401 (2016).
25. Chowdhury, B. *et al.* Salen type ligand as a selective and sensitive nickel (II) ion chemosensor: A combined investigation with experimental and theoretical modelling. *Sens. Actuators B Chem.* **276**, 560–566 (2018).
26. Santhi, S., Amala, S., Renganathan, R., Subhashini, M. & Basheer, S. Colorimetric and fluorescent sensors for the detection of Co (II), Ni (II) and Cu (II) in aqueous methanol solution. *Res. Chem. Intermed.* **45**, 4813–4828 (2019).
27 Reissert, A. Ueber Di-(γ-amidopropyl) essigsäure (Diamino. 1.7. heptanmethylsäure. 4) und ihr inneres Condensationsproduct, das Octohydro. 1.8. naphtyridin. *Ber. Dtsch. Chem. Ges.* **26**, 2137–2144 (1893).
28 Bobrański, B. & Sucharda, E. Über eine Synthese des 1.5-Naphthyridins. *Berichte der deutschen chemischen Gesellschaft (A and B Series)* **60**, 1081–1084 (1927).
29. Schmitz, F. J., DeGuzman, F. S., Hossain, M. B. & Van der Helm, D. Cytotoxic aromatic alkaloids from the ascidian *Amphicarpa meridiana* and *Leptoclinides* sp.: Meridine and 11-hydroxyascididemin. *J. Org. Chem.* **56**, 804–808 (1991).
30. Tejeria, A. *et al.* Antileishmanial effect of new indeno-1, 5-naphthyridines, selective inhibitors of *Leishmania infantum* type IB DNA topoisomerase. *Eur. J. Med. Chem.* **124**, 740–749 (2016).
31. Schmitz, F. J., Agarwal, S. K., Gunasekera, S. P., Schmidt, P. G. & Shoolery, J. N. Amphimedine, new aromatic alkaloid from a pacific sponge, *Amphimedon* sp. Carbon connectivity determination from natural abundance carbon-13-carbon-13 coupling constants. *J. Am. Chem. Soc.* **105**, 4835–4836 (1983).
32. Goutham, K., Kadiyala, V., Sridhar, B. & Karunakar, G. V. Gold-catalyzed intramolecular cyclization/condensation sequence: Synthesis of 1, 2-dihydro [c][2,7] naphthyridines. *Org. Biomol. Chem.* **15**, 7813–7818 (2017).
33. Qu, L., Yin, C., Huo, F., Zhang, Y. & Li, Y. A commercially available fluorescence chemosensor for copper ion and its application in bioimaging. *Sens. Actuators B Chem.* **183**, 636–640 (2013).
34. Zhu, Y. *et al.* A reversible fluorescent chemosensor for the rapid detection of mercury ions (II) in water with high sensitivity and selectivity. *RSC Adv.* **4**, 61320–61323 (2014).
35. Yao, D., Huang, X., Guo, F. & Xie, P. A new fluorescent enhancement chemosensor for Al^{3+} and Fe^{3+} based on naphthyridine and benzothiazole groups. *Sens. Actuators B Chem.* **256**, 276–281 (2018).
36. Udhayakumari, D., Velmathi, S., Sung, Y.-M. & Wu, S.-P. Highly fluorescent probe for copper (II) ion based on commercially available compounds and live cell imaging. *Sens. Actuators B Chem.* **198**, 285–293 (2014).
37. Ashraf, A., Shafiq, Z., Mahmood, K., Yaqub, M. & Rauf, W. Regioselective, one-pot, multi-component, green synthesis of substituted benzo[c]pyrazolo [2,7]naphthyridines. *RSC Adv.* **10**, 5938–5950 (2020).
38. Jiang, J., Gou, C., Luo, J., Yi, C. & Liu, X. A novel highly selective colorimetric sensor for Ni (II) ion using coumarin derivatives. *Inorg. Chem. Commun.* **15**, 12–15 (2012).
39. Son, Y.-A., Gwon, S.-Y. & Kim, S.-H. A colorimetric and fluorescent chemosensor for Ni^{2+} based on donor-π-acceptor charge transfer dye containing 2-cyanomethylene-3-cyano-4, 5, 5-trimethyl-2, 5-dihydrofuran acceptor and 4-bis (pyridin-2-ylmethyl) aminobenzene donor. *J. Nanosci. Nanotechnol.* **12**, 1503–1506 (2012).
40. Job, P. Job's method of continuous variation. *Ann. Chim* **9**, 113 (1928).
41. Benesi, H. A. & Hildebrand, J. A spectrophotometric investigation of the interaction of iodine with aromatic hydrocarbons. *J. Am. Chem. Soc.* **71**, 2703–2707 (1949).
42. Kang, J. H., Lee, S. Y., Ahn, H. M. & Kim, C. A novel colorimetric chemosensor for the sequential detection of Ni^{2+} and CN− in aqueous solution. *Sens. Actuators B Chem.* **242**, 25–34 (2017).
43. Committee, A. M. Recommendations for the definition, estimation and use of the detection limit. *Analyst* **112**, 199–204 (1987).
44. Dhanushkodi, M. *et al.* A simple pyrazine based ratiometric fluorescent sensor for Ni^{2+} ion detection. *Dyes Pigm.* **173**, 107897. https://doi.org/10.1016/j.dyepig.2019.107897 (2020).
45. Liu, Y.-L. *et al.* A new fluorescent chemosensor for Cobalt (II) ions in living cells based on 1,8-naphthalimide. *Molecules* **24**, 3093 (2019).
46. Kumar, G. G. V. *et al.* A Schiff base receptor as a fluorescence turn-on sensor for Ni^{2+} ions in living cells and logic gate application. *New J. Chem.* **42**, 2865–2873 (2018).
47 Lever, A. B. P. The magnetic moments of some tetragonal nickel complexes. *Inorg. Chem.* **4**, 763–764 (1965).
48 Fang, L. *et al.* Experimental and theoretical evidence of enhanced ferromagnetism in sonochemical synthesized BiFeO$_3$ nanoparticles. *Appl. Phys. Lett.* **97**, 242501 (2010).

49. Weigend, F. & Ahlrichs, R. Balanced basis sets of split valence, triple zeta valence and quadruple zeta valence quality for H to Rn: Design and assessment of accuracy. *Phys. Chem. Chem. Phys.* **7**, 3297–3305 (2005).
50. Frisch, M. & Clemente, F. Gaussian 09, Revision A. 01, MJ Frisch, GW Trucks, HB Schlegel, GE Scuseria, MA Robb, JR Cheeseman, G. Scalmani, V. Barone, B. Mennucci, GA Petersson, H. Nakatsuji, M. Caricato, X. Li, HP Hratchian, AF Izmaylov, J. Bloino, G. Zhe (2009).
51. Bader, R. (Oxford, UK, 1994).
52. Popelier, P. L. A., Aicken, F. & O'Brien, S. *Atoms in Molecules* (Prentice Hall, Manchester, 2000).
53. Kumar, P. S. V., Raghavendra, V. & Subramanian, V. Bader's theory of atoms in molecules (AIM) and its applications to chemical bonding. *J. Chem. Sci.* **128**, 1527–1536 (2016).
54. Lu, T. & Chen, F. Multiwfn: a multifunctional wavefunction analyzer. *J. Comput. Chem.* **33**, 580–592 (2012).
55. Humphrey, W., Dalke, A. & Schulten, K. VMD: Visual molecular dynamics. *J. Mol. Graph.* **14**, 33–38 (1996).
56. Zhao, Y. & Truhlar, D. G. The M06 suite of density functionals for main group thermochemistry, thermochemical kinetics, noncovalent interactions, excited states, and transition elements: Two new functionals and systematic testing of four M06-class functionals and 12 other functionals. *Theoret. Chem. Acc.* **120**, 215–241 (2008).
57. Neese, F. The ORCA program system. *Wiley Interdisciplinary Reviews: Computational Molecular Science* **2**, 73–78 (2012).

Acknowledgements

Author contributions

A.A. carried out synthesis of probes and write up; M.I. and A.S. did calorimetric and fluorescence analysis; M.T.A. and A.H.B. performed ICPOES, SEM and analytical applications; M.K. and A.M.E carried out DFT/computational studies and prepared figures; Z.S., A.P.D. and M.Y. designed concept of study and wrote/revised the main manuscript.

Competing interests

The authors declare no competing interests.

Additional information

Supplementary Information The online version contains supplementary material available at https://doi.org/10.1038/s41598-021-98400-2.

Correspondence and requests for materials should be addressed to M.K. or Z.S.

Reprints and permissions information is available at www.nature.com/reprints.

Publisher's note Springer Nature remains neutral with regard to jurisdictional claims in published maps and institutional affiliations.